Journal of Materials Science: Materials in Electronics (2019) 30:10686–10693
https://doi.org/10.1007/s10854-019-01414-w

Dielectric, ferroelectric and electromechanical properties of $(1-x)(Bi_{0.5}Na_{0.5}TiO_3–xBa(Ti_{0.8}Zr_{0.2})O_3$ ceramics

Muhammad Javid Iqbal[1] · Amir Ullah[2] · Ihsan Ur Rehman[1] · Aman Ullah[3] · Yaseen Iqbal[4] · Ill Won Kim[5]

Received: 7 February 2019 / Accepted: 25 April 2019 / Published online: 30 April 2019

Abstract
Piezoelectric ceramic compounds in the $(1-x)Bi_{0.5}Na_{0.5}TiO_3–xBaZr_{0.8}Ti_{0.2}O_3$ (BNT–*x*BZT) with $x=0$–0.05 solid solution series were made by solid-state-reaction method. X-ray diffraction (XRD) of (BNT–*x*BZT) revealed rhombohedral symmetry for all BZT ratios up to $x=0.04$ and changed to tetragonal symmetry for BZT ratio 0.05. Moreover, enhancement in the volume of unit cell with the increasing of BZT ratio was also detected. Scanning electron microscopy demonstrated a variation in the average grain size with increasing in BZT concentration. Dielectric measurements displayed a steady enhancement in the dielectric constant with increase in doping up to ratio $x=0.02$ and decreased with increasing in BZT amount. In polarization study the remnant polarization and coercive field was decreased with increasing BZT doping. The strain was increased with the increasing of BZT content and maximum strain of 0.20% was found for $x=0.05$.

1 Introduction

Lead based piezoceramics such as $Pb(Zr_xTi_{1-x})O_3$ (PZT) are known for their attractive piezoelectric properties, and hence, the relevant applications. These materials are toxic because of high lead content despite their excellent properties; therefore, extensive efforts are being made to fabricate and develop Pb-free piezoelectric ceramics having properties similar to those of Pb-based ceramics [1]. The investigation of Pb-free ceramics with excellent properties attracted vital interest, so relatively more attention is focused to investigate and study Pb-free piezoceramics [2].

Bismuth based perovskite ceramics such as $(Bi_{1/2}Na_{1/2})TiO_3$ (BNT) having a rhombohedral structure was supposed to be one of the possible Pb-free candidates due to their excellent ferroelectric features (P_r of 38 μC/cm^2 and $E_c=73$ kV/cm) and also with a large Curie temperature (T_c) value 320 °C [1–10]. BNT exhibited an anomalous dielectric behavior which displayed a phase transition from the ferroelectric to anti-ferroelectric at low-temperature ~ 200 °C, known as depolarization temperature (T_d) [5–11]. Furthermore, the electromechanical properties of BNT are worse than those of lead-based ceramics. BNT ceramics cannot be poled easily because of its high E_c (73 kVcm). Solid solutions of BNT with barium titanate, $BaTiO_3$ (BT) [11], bismuth potassium titanate $(Bi_{1/2}K_{1/2})TiO_3$ (BKT) [12] and cerium dioxide doped barium titanate, $BaTiO_3+CeO_2$ [13] have resulted in better piezoelectric properties along with the easier poling process than that of pure BNT. However, the strain properties were found still too weak and were suitable for practical applications unless T_d is decreased considerably.

BNT–xBKT (x = 0.16–0.20 mol) ceramics have been studied and found interesting due to their morphotropic phase boundary (MPB) in the transition from rhombohedral (F_R) to tetragonal (F_T) phase [12, 14]. Also, BNT-BKTs exhibited relatively better piezoelectric, ferroelectric and dielectric properties near the MPB composition, along with a comparatively higher depolarization temperature T_d.

✉ Amir Ullah
aamiru8@gmail.com

✉ Ill Won Kim
kimiw@ulsan.ac.kr

[1] Department of Physics, University of Peshawar, Peshawar 25120, KP, Pakistan

[2] Department of Physics, Islamia College Peshawar, Peshawar 25120, KP, Pakistan

[3] Department of Physics, University of Science and Technology, Bannu, KP, Pakistan

[4] Materials Research Laboratory, Department of Physics, University of Peshawar, Peshawar 25120, Pakistan

[5] Department of Physics and Energy Harvest Storage Research Center (EHSRC), University of Ulsan, Ulsan 680-749, Republic of Korea

Pb-free barium strontium titanate $(Ba_{1-x}Sr_x)TiO_3$ and doped $BaTiO_3$ are now being considered potential candidate dielectrics regarding capacitor applications [14]. The main reason for adding Sr^{2+} to $BaTiO_3$ is to shift the T_d by approximately 130 °C towards room temperature (RT), displaying a high dielectric constant and low tangent loss (tanδ) [12]. Lee et al. [15] investigated Pb-free $(1-x)(Bi_{0.5}Na_{0.5})TiO_3$–$x(Ba_{0.7}Sr_{0.3})TiO_3$ ceramic systems and reported that the incorporation of $(Ba_{0.7}Sr_{0.3})TiO_3$ into $(Bi_{0.5}Na_{0.5})TiO_3$ caused a rhombohedral to tetragonal phase transition. Moreover, enhancements in both dielectric and piezoelectric properties were reported at ratio, $x=0.08$ (MPB).

Usually, the properties of piezoelectric materials can be effectively improved by multicomponent systems [16]. Song et al. [17] reported interesting piezoelectric properties in the MPB region for BNT-BT and BKT-BNT ceramics, but the depolarization temperature T_d was decreased by 100 °C in the MPB region. This decrease in the T_d was considered as a big problem in the way of Pb-free piezoelectric ceramics to be used in practical applications. These studies demonstrate that binary systems do not have the ability to fully replace Pb-based piezoelectrics. Consequently, research efforts are being focused on the fabrication of new compositions using ternary systems which permit more degrees of freedom than the binary systems [18].

Previously, BNKLT and (Bi,Na,Li)TiO_3 systems were doped with BZT and the effect of dopant on dielectric and piezoelectric properties was studied [19, 20]. Similarly, in another report, BNT was also doped with modifier Ba^{2+} and Zr^{4+}, however, these studies are limited to only dielectric analysis [21]. Therefore, a perovskite modifier $Ba(Ti_{0.8}Zr_{0.2})O_3$ of ratios of Ti(0.8) and Zr(0.2) was thus selected for BNT due to its scant research reports and non-availability of detail study regarding dielectric properties, electric field dependent polarization and strain response of BNT-BZT ceramics. Moreover, BZT was considered to enhance the dielectric, ferroelectric and strain properties of BNT by modifying the internal symmetry of lattice of the system. The solid solution series of $(1-x)\ Bi_{0.5}Na_{0.5}TiO_3$–$xBaZr_{0.8}Ti_{0.2}O_3$, $(1-x)$ BNT–xBZT ($x=0$, 0.01, 0.02, 0.03, 0.4, and 0.05) Pb-free ceramics were made. The influence of BZT addition on the structure, dielectric, ferroelectric and electromechanical properties of the resulting ceramics was investigated and discussed.

2 Experimental

Pb-free $(1-x)Bi_{0.5}Na_{0.5}TiO_3$–$xBaZr_{0.8}Ti_{0.2}O_3$ (BNT–BZT) ($x=0$–0.05) ceramic systems were fabricated via a solid-state-reaction technique. Bi_2O_3, Na_2CO_3, TiO_2 (99.9% High Purity Chemicals, Japan), ZrO_2, and $BaCO_3$ (99.9% Cerac Specialty In-organics, USA) were the starting ceramic powders. Weighing of the initial ingredients was done according to the stoichiometric proportions and then followed by ball milling step for 24 h in ethanol with Yt-toughened zirconia balls. The prepared batches were dried at 100 °C followed by re-grinding. The finely ground powders were calcined at 850 °C for 2 h at a heating/cooling rate of 5 °C/min. The powdered calcined samples were again milled for 24 h. An aqueous polyvinyl alcohol (PVA) solution was mixed in these calcined powders and green disks of diameter 10 mm were pressed at a pressure of 120 MPa. The disks were sintered in closed alumina crucibles at temperature 1170–1180 °C for 2 h at a heating and cooling rate of 5 °C/min. Sintered disks were polished, and the phase structure and lattice parameters of the constituent phase(s) were found by a X' Pert-PRO, MRD, Philips, KBSI X-ray diffractometer (XRD).

In order to remove the rough surface, lapping was performed for microstructural study. The lapped disks were again carefully polished and then thermally etched at 1050 °C for 30 min. Scanning electron microscopy (SEM, JSM5910, Japan) was used to study the microstructure of the as thoroughly polished disks. Both the surfaces of these disks were electroded with silver paste. The electroded/silver pasted surfaces were cooked at temperature 700 °C for 1 h. The *P–E* loops were recorded in silicon oil by a Sawyer–Tower circuit. The strain was found using a linear-variable-differential-transducer (LVDT, Mitutoyo MCH-331 & M401).

For dielectric measurements, all the disks were polled in silicon oil by an external electric field 30–40 kV/cm for 30 min and the dielectric constant was determined by an impedance analyzer (HP4192A).

3 Results and discussion

Figure 1 shows the XRD patterns of $(1-x)$BNT–xBZT compositions with $x=0$–0.05. Analysis of XRD patterns revealed that these samples crystallized into a perovskite rhombohedral structure for the samples $0\le x\le 0.04$ and transformed into tetragonal for $x=0.05$. Additionally, it was detected that all the samples formed a single phase compounds with no evidence of secondary phase(s). This shows that the BZT ceramics diffused fully into the BNT crystals to make a homogenous solid solution. Furthermore, XRD peaks were observed slightly shifted towards lower 2θ values displaying an enhancement in the volume of unit cell because of the substitution of smaller ionic radii Bi^{3+} (1.03 Å) and Ti^{4+} (0.605 Å) with the relative larger ionic radii Ba^{2+} (1.35 Å) and Zr^{4+} (0.72 Å), respectively.

The widening of (111) and (200) peaks suggest the presence of rhombohedral structure for $0\le x\le 0.04$. However, for $x=0.05$, the crystal structure was transformed to the

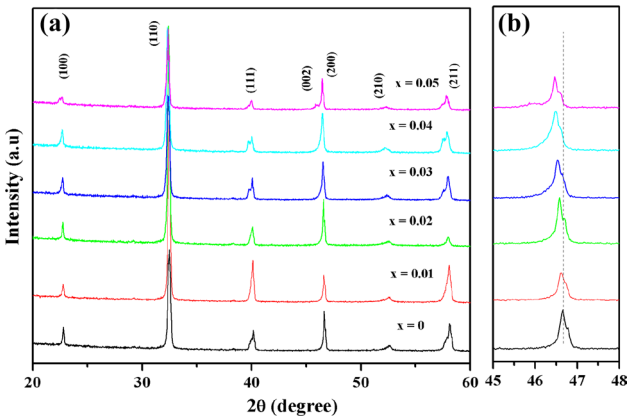

Fig. 1 XRD patterns of sintered (1 − x)BNT–xBZT (x = 0, 0.01, 0.02, 0.03, 0.04 and 0.05) ceramics

tetragonal structure as can be evidenced by the splitting of (200) peak around 2θ = 46°. The observed crystal symmetry was in agreement to the previously reported studies [22–24].

Figure 2 displays the SEM figures of sintered (1 − *x*) BNT–*x*BZT ceramics. The sample has nonuniform and porous morphology and with inhomogeneous grains but with clear grain boundaries. The microstructure of the undoped sample i.e., pure BNT was comprised of irregular-shaped grains of dimensions ranging from 3 to 12 µm with average grain size of 7.5 µm. For sample $x = 0.01$, the dimensions of some of the grains were to increase up to ~ 40 µm; however, some small grains (~ 3 µm in size) could still be seen. When BZT concentration was further increased e.g. to 0.02 and 0.03, the microstructure appeared relatively more uniform and the average grain size decreased to about 5 µm. For $x = 0.04$, the mean grain size was found to increase to about 10 µm. With further enhancement in *x*, the mean grain size

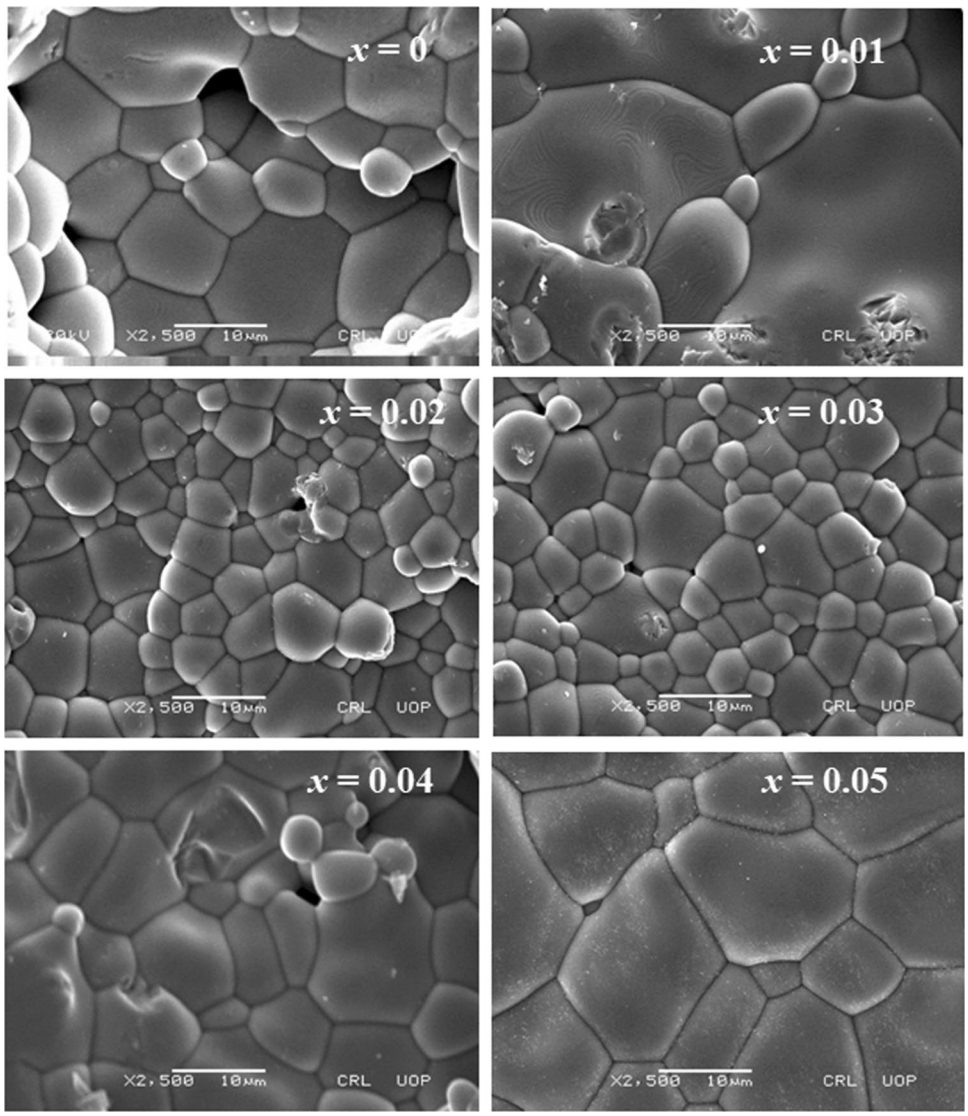

Fig. 2 SEM micrographs of (1 − x)BNT–xBZT (x = 0, 0.01, 0.02, 0.03, 0.04 and 0.05) ceramics

again decreased to around ~ 6 μm for the composition with $x = 0.05$.

Figure 3 displays the temperature dependent dielectric constant and dielectric loss of $(1 - x)$BNT–xBZT ($x = 0$, 0.01, 0.02, 0.03, 0.04, and 0.05) ceramics at frequencies 1 kHz, 10 kHz and 100 kHz. Two peaks could be found in the dielectric graphs for each sample in agreement to those found in reported literature [25–27].

The observed peaks could be ascribed to the temperature of depolarization (T_d) of the dipoles and the maximum temperature (T_m) associated with the maximum value of dielectric constant. The values of T_d and T_m were noted to decrease with increasing of BZT content, which indicated that conductivity of these ceramics decreased in comparison with the pure BNT ceramics. Moreover, dielectric constant increased with an enhancement in BZT concentration up to $x = 0.02$ and then decreased upon further addition of the BZT concentration. The observed trend can be due to the replacement of Na (186 pm), Bi (156 pm), and Ti (147 pm) ions by Ba and Zr ions having ionic radii 222 and 160 pm, respectively [28, 29]. Meanwhile, BNT–BZT ceramics leads to a decrease in dielectric constant because of the possible reaction of oxygen vacancies (VO) with doping of BZT ceramics. When the BZT ratio touches its limit, further incorporation saturates the BNT lattice matrix and results in the clamping of the domain walls [28–30]. This clamping will restrain the macro–micro domain switching to some degree; this is the reason that the relative permittivity declines. Bothe the T_m and T_d shifts to lower temperature with the increasing of ratio x. T_m drops from 298 °C to 254 °C for $0 \le x \le 0.05$. The permittivity peak became broader and smoothly varied with temperature with an increase in x. The diffuseness in the permittivity peak is due to the chemical heterogeneity due to the more disorderdness of A and B-sites, hence, unit cells have dissimilar values of T_c. The T_d almost vanished for the higher ratios of the BZT ($x \ge 0.04$).

The dielectric loss (tan δ) first enhanced with an enhancement in temperature and showed a hump at T_d and then drops until reaching T_m suggests less distortion of the crystal structure. Above T_m, the tan δ increased abruptly which may be ascribed to the rise in conductivity with the increase in temperature due to the volatility of Bi^{3+}. The sharp increase in dielectric constant at high temperatures for the lower amount of BZT may be suggested due to an increase in conductivity, because the poor morphology and volatility of Bi^{3+} cations creates oxygen vacancies for neutralization of charge. When the amount of x is increased, Bi^{3+} cation is replaced by less volatile Ba^{2+}, and hence tan δ decreases.

Figure 4 shows the ferroelectric (P–E) hysteresis loops of the $(1 - x)$BNT–xBZT ($x = 0$, 0.01, 0.02, 0.03, 0.04, and 0.05) ceramics. The undoped sample displayed a normal P–E hysteresis loop with a P_r of 31 μC/cm^2 and an E_c of 46.0 kV/cm. It is evident that BZT affected the shape of hysteresis loop and the values of polarization up to $x = 0.05$. The coercive field E_c and P_r steadily decreased with increasing BZT content and for $x = 0.05$, E_c and P_r reached the minimum value of 31 kV/cm and 22 μC/cm^2, respectively. This decrease in E_c and P_r, along with a simultaneous decrease in maximum polarization, P_m, suggested that the high ferroelectric trend, prevailing in BNT, was disturbed with the

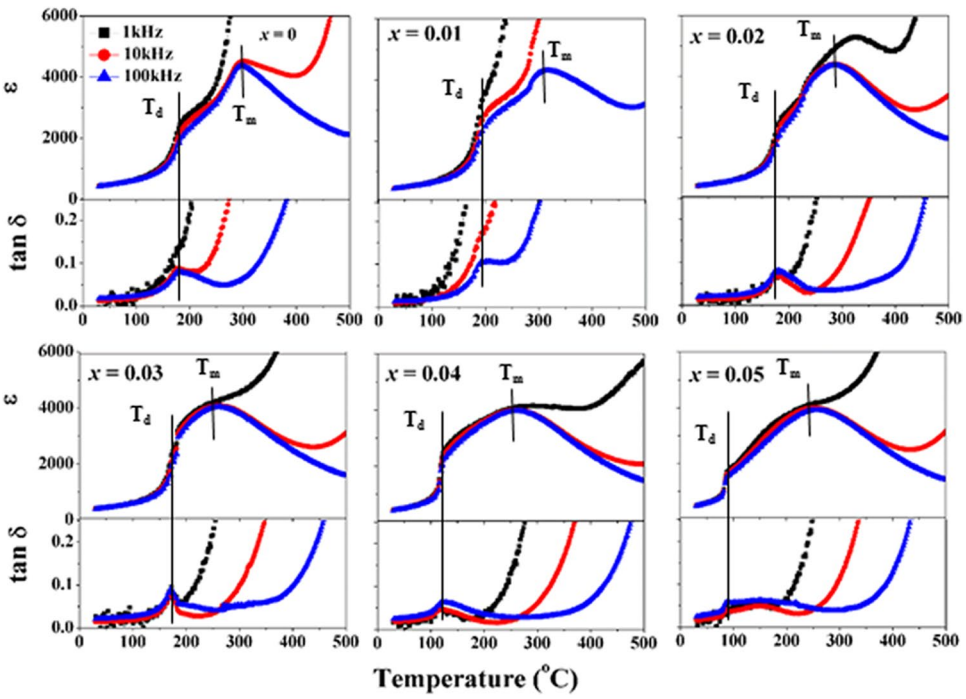

Fig. 3 Dielectric constant and loss of (1 − x)BNT–xBZT ($x = 0$, 0.01, 0.02, 0.03, 0.04 and 0.05) ceramics at selected frequencies 1, 10 and 100 kHz

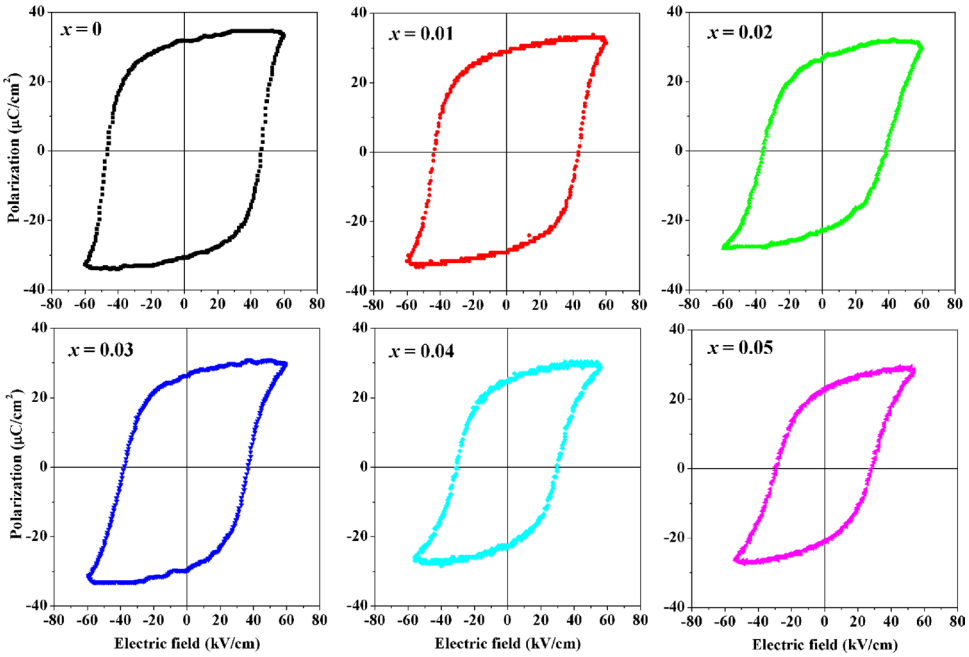

Fig. 4 P-E hysteresis loops of the (1 − x)BNT–xBZT (x = 0, 0.01, 0.02, 0.03, 0.04, and 0.05) ceramics

incorporation of BZT. The polarization was strongly affected by BZT concentration, external field and domain orientation, which ultimately contributed to the material response. Identical oriented domain structure actually increases the dielectric properties. For $x = 0$, $(1 - x)$BNT–xBZT ceramics have a large value of P_r; which exhibits the presence of a relatively better uniform structure of domains [31–35].

Figure 5 displays the loops of bipolar stain of (1 − x) BNT–xBZT ceramics also named as a butterfly loop obtained at frequency of 200 mHz. All the $(1 - x)$ BNT–xBZT ($0 \le x \le 0.05$) compositions showed the characteristic ferroelectric butterfly-shaped loops.

The undoped sample showed a normal butterfly-shaped bipolar strain hysteresis loop with a maximum strain (S_{max}) of 0.09%. A negative strain (S_{neg}) (that displays the difference between the strain at zero electric field and the lowest strain which can be only visible in the bipolar cycle) [36, 37] of ~ 0.15% was recorded for undoped BNT. The maximum strains were recorded to be 0.11, 0.15, 0.16, 0.20, and 0.16% for the $x = 0$, 0.01, 0.02, 0.020, 0.03, 0.04 and

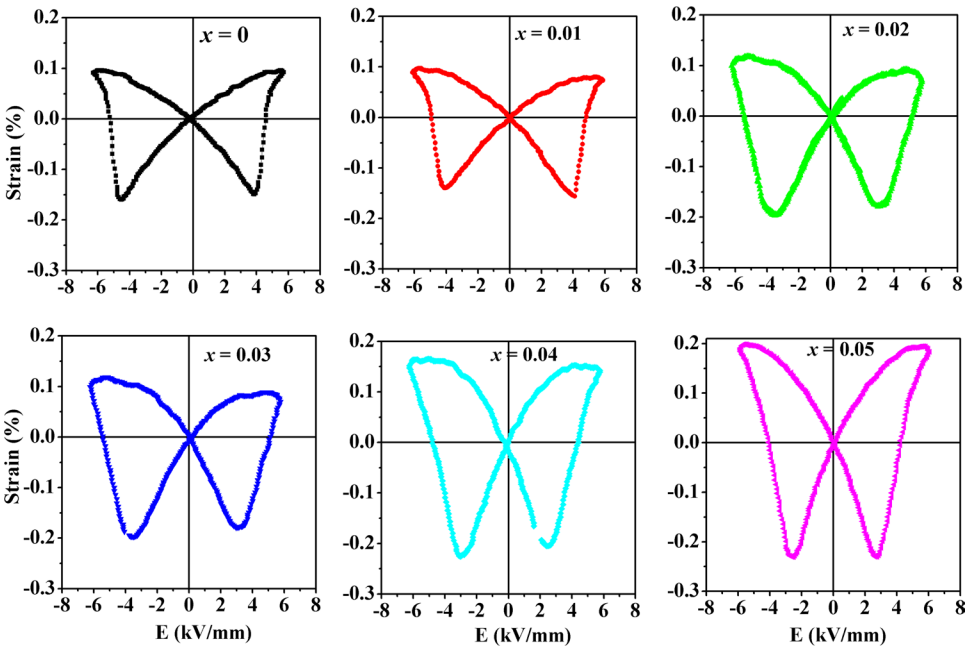

Fig. 5 Bipolar strain loop of $(1 - x)$BNT–xBZT (x = 0, 0.01, 0.02, 0.03, 0.04 and 0.05) ceramics at maximum electric field of 60 kV/cm

0.05 compositions, respectively. The largest S_{max} (~0.20%) was obtained at $x=0.05$ which may be ascribed to the low E_c ~ 34 kV/cm and small P_r ~ 24 μC/cm^2, large grain size and high density. The increase in S_{max} of $x=0.05$ composition may be due to the change in the crystal structure from rhombohedral to tetragonal. The loops display a steady change from the typical ferroelectric to a slight relaxer-like behavior with increasing BZT content. For all samples, the negative strain persisted and increased with the dopant (BZT) concentration. The loops display a steady change from typical ferroelectric to a slight relaxor behavior as BZT ratio is increased. In all samples, the negative strain remains and increased with doping of BZT amount.

Figure 6 shows the electric field induced unipolar strain hysteresis of $(1-x)$BNT–xBZT ceramics ($x=0$, 0.01, 0.02. 0.04 and 0.05), with a maximum electric field of 60 kV/cm. The increase of total strain was found to behave as like of polarization behavior (Fig. 4). The polarization loops found to be more saturated, and the strain loops also displayed by all the samples in a similar way. The strain increased with BZT concentration up to $x=0.05$, and in similar fashion as that of the bipolar strain loops. The dynamic electric field induced strain, (d^*_{33}), obtained from S_{max}/E_{max}, was 325 pm/V for $x=0.05$, with a drop in the E_c, consistent with the previous studies as reported in literature [38, 39].

The comparisons of the S_{max}/E_{max} vs. hysteresis ($\Delta S/S_{max}$) in the unipolar S–E loop for various BNT-based ceramics are displayed in Fig. 7. The largest S_{max}/E_{max} of value 727 pm/V for Li- and Ta-doped BNKT was reported with a hysteresis that reached 70% [40]. Hysteresis loss can be decreased by lowering the value of S_{max}/E_{max}. Therefore, in current studies

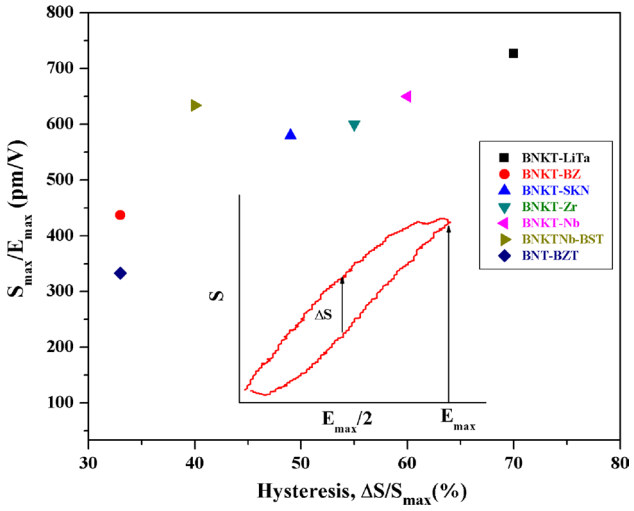

Fig. 7 Comparison of normalized strain coefficient (S_{max}/E_{max}) versus hysteresis ($\Delta S/S_{max}$) for different BNT-based systems: BNKT-LiTa [40], BNKT-BZ [41], BNKT-SKN [42], BNKT-Zr [43], BNKT-Nb [44], BNKTNb-BST [8] and those of the current study BNT–BZT ceramics

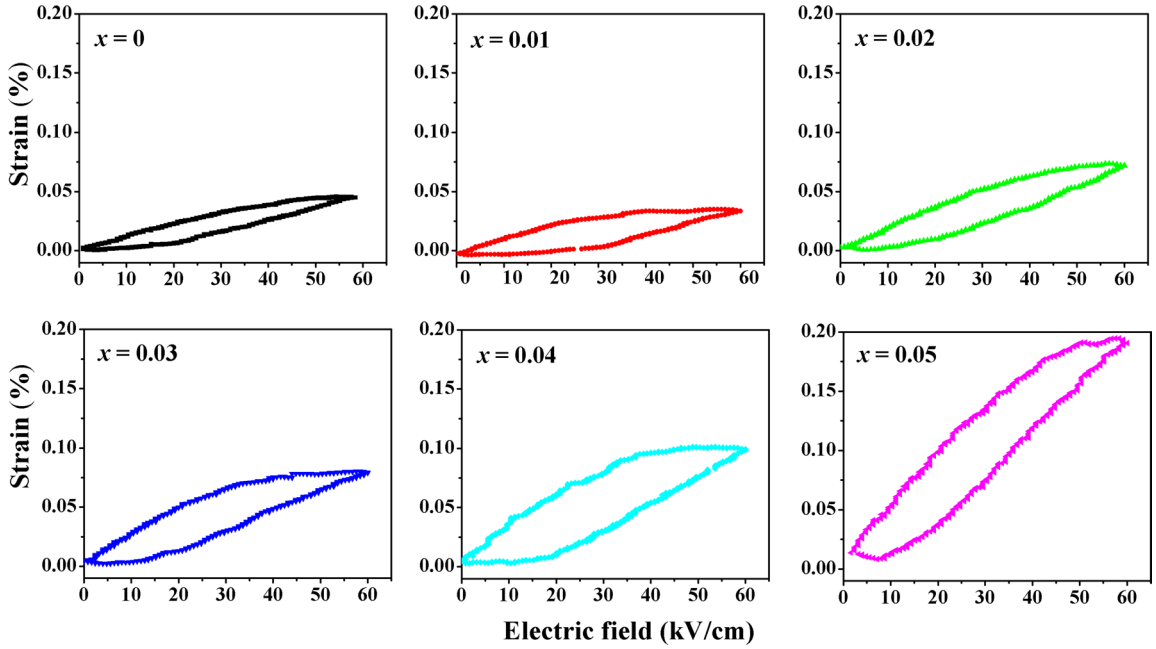

Fig. 6 Unipolar strain hysteresis loops of $(1-x)$BNT–xBZT ($x=0$, 0.01, 0.02, 0.03, 0.04 and 0.05) at maximum electric field of 60 kV/cm

a normalized strain of 333 pm/V with a relatively low hysteresis loss of 33% was achieved.

4 Conclusions

$(1-x)Bi_{0.5}Na_{0.5}TiO_3$–$xBaZr_{0.8}Ti_{0.2}O_3$ (1 − x)BNT–xBZT (x = 0–0.05) piezoelectrics were fabricated via a solid-state-reaction method. XRD analysis revealed the single phase rhombohedral perovskite at $0 \le x \le 0.04$ which transformed to the tetragonal structure at $x = 0.05$. Microstructural analysis presented that the morphology and density of the (1 − x) BNT–xBZT compound improved with enhancing of BZT contents. For $x = 0.02$ and 0.03, the grain size was observed to be decreased while at $x = 0.05$, the average grain size was increased to ~ 10 μm. Analysis of the temperature and frequency dependent dielectric constant exhibited that T_d and T_m drops with enhancing of dopand amount. For $x \ge 0.04$, the T_d almost vanished. The T_m decreased from 298 °C for $x = 0$ to 254 °C for $x = 0.05$ and the permittivity peak became more diffused. The polarization of the ceramics shows a decrease in E_c from 46 kV/cm for $x = 0$ to 28 kV/cm for $x = 0.05$ which may be due to the replacement of active Ti^{4+} with inactive Zr^{4+} that inhibited the creation of high ferroelectric domains. The minimum P_r (~ 22 μC/cm^2) with the lowest E_c (~ 31 kV/cm^2) were found at $x = 0.05$. The S_{max} enhanced from ~ 0.04% for $x = 0$ to ~ 0.20% for $x = 0.05$ that could be suggested due to the low E_c, small P_r and large grain size. The bipolar stain showed the same behavior for all the investigated samples and was maximum at $x = 0.05$. The x = 0.05 composition was observed to exhibit favorable properties, such as low E_c (~ 34 kV/cm^2), large P_r (~ 24 μC/cm^2) with high S_{max} (~ 0.20%), will be very useful for actuators.

Acknowledgements This work was supported by a National Research Foundation of Korea (NRF) grant funded by the Korea government Ministry of Education (No. NRF-2017 R1D1A1B03036032).

References

1. T.R. Shrout, S.J. Zhang, J. Electroceram. **19**, 111 (2007)
2. S.H. Choy, X.X. Wong, H.L.W. Chan, C.L. Choy, Appl. Phys. A **89**, 775 (2007)
3. A. Safari, E.K. Akdog, *Piezoelectric acoustic materials for transducer Applications* (Springer, New York, 2008)
4. L. Egerton, D.M. Dillon, J. Am. Ceram. Soc. **42**, 438 (1959)
5. A. Ullah, A. Ullah, M.J. Iqbal, M.N. Khalid, A. Ali, A. Zeb, T. Khan, I.W. Kim, J. Mater. Sci. Mater. Electron. **28**, 8397–8404 (2017)
6. A. Ullah, H.B. Gul, A. Ullah, M. Sheeraz, J.S. Bae, W. Jo, C.W. Ahn, I.W. Kim, T.H. Kim, APL Mater. **6**, 016104 (2018)
7. M. Ullah, H.U. Khan, A. Ullah, A. Ullah, I.W. Kim, I. Qazi, I. Ahmad, Ceram. Int. **44**, 556–562 (2018)
8. A. Ullah, R.A. Malik, A. Ullah, D.S. Lee, S.J. Jeong, J.S. Lee, I.W. Kim, C.W. Ahn, J. Eur. Ceram. Soc. **34**, 29–35 (2014)
9. A. Ullah, M. Alam, A. Ullah, C.W. Ahn, J.S. Lee, S. Cho, I.W. Kim, RSC Adv. **6**, 63915 (2016)
10. A. Ullah, M. Rahman, M.J. Iqbal, C.W. Ahn, I.W. Kim, A. Ullah, J. Korean Phys. Soc. **68**(12), 1455–1460 (2016)
11. T. Takenaka, K. Maruyama, K. Sakata, Jpn. J. Appl. Phys. Part 1 **30**, 2236 (1991)
12. A. Sasaki, T. Chiba, Y. Mamiya, E. Otsuki, Jpn. J. Appl. Phys. Part 1 **38**, 5564 (1999)
13. X. Wang, H.L.W. Chan, C.L. Choy, Sol. Stat. Commun. **125**, 395 (2003)
14. D.E. Rase, R. Roy, J. Am. Ceram. Soc. **38**, 102 (1955)
15. W.C. Lee, C.Y. Huang, L.K. Tsao, Y.C. Wu, J. Alloy. Compd. **492**, 307 (2010)
16. H. Nagata, J. Ceram. Soc. Jpn. **116**(1350), 271–277 (2008)
17. T. Song et al., J. Korean Phys. Soc. **51**, 697 (2007)
18. E. Aksel, J.L. Jones, Sensors **10**(3), 1935–1954 (2010)
19. Z. Zhang, J. Jia, H. Yang, C. Chen, H. Sun, X. Hu, D. Yang, J. Mater. Sci. **43**, 1501 (2008)
20. Y. Huang, Y. Liu, L. Gao, T. Liu, G. Zhang, J. Mater. Sci. Mater. Electron. **21**, 1055–1059 (2010)
21. A. Hussain, J.U. Rahman, A. Maqbool, M.S. Kim, T.K. Song, W.J. Kimand, M.H. Kim, Phys. Status Solidi A **211**, 1704 (2014)
22. C.H. Wang, J. Ceram. Soc. Jpn **116**, 632–636 (2008)
23. B. Parija, T. Badapanda, S.K. Rout, L.S. Cavalcante, S. Panigrahi, E. Longo, N.C. Batista, T.P. Sinha, Ceram. Int. **39**, 4877–4886 (2013)
24. F. Guo, B. Yang, S. Zhang, F. Wu, D. Liu, P. Hu, Y. Sun, D. Wang, W. Cao, Appl. Phys. Lett. **103**, 182906 (2013)
25. A. Ullah, M. Ullah, A. Ullah, A. Ullah, G. Sadiq, B. Ullah, A. Zeb, S.U. Jan, I.W. Kim, J. Korean Phys. Soc. **34**, 589–594 (2019)
26. D. Li, Z.Y. Shen, Z. Li, X. Wang, W.Q. Luo, F. Song, Z. Wang, Y. Li, J. Mater. Sci. Mater. Electron. **30**, 5917–5922 (2019)
27. M. Xiao, H. Sun, Y. Wei, L. Li, P. Zhang, J. Mater. Sci. Mater. Electron. **29**, 17689–17694 (2018)
28. R.D. Shannon, C.T. Prewitt, Acta Crystallogr. **25**, 925 (1969)
29. W.C. Lee, C.Y. Huang, L.K. Tsao, Y.C. Wu, J. Alloys Compd. **492**, 307 (2010)
30. A. Rachakom, P. Jaiban, S. Jiansirisomboon, A. Watcharapasorn, NanoRes. Lett. **7**, 57 (2012)
31. E.R. Leite, A.M. Scotch, A. Khan, T. Li, H.M. Chan, M.P. Harmer, S.F. Liu, S.E. Park, J. Am. Ceram. Soc. **85**, 3018–3024 (2002)
32. M. Chen, Q. Xu, B.H. Kim, B.K. Ahn, J.H. Ko, W.J. Kang, O.J. Nam, J. Eur. Ceram. Soc. **28**, 843 (2008)
33. Z. Yang, B. Liu, L. Wei, Y. Hou, Mater. Res. Bull. **43**, 81 (2008)
34. Q. Zhou, C. Zhou, W. Li, J. Cheng, H. Wang, C. Yuan, J. Phys. Chem. Sol. **72**, 909 (2011)
35. C. Zhou, X. Liu, W. Liu, C. Yuan, J. Phys. Chem. Sol. **70**, 541 (2009)
36. P. Jaita, A. Watcharapasorn, S. Jiansirisomboon, Nano Res. Lett. **7**, 24 (2012)
37. A. Ullah, C.W. Ahn, R.A. Malik, J.S. Lee, I.W. Kim, J. Electroceram. **33**, 187–194 (2014)
38. J. Chen, X.L. Tan, W. Jo, J. Rödel, J. Appl. Phys. **106**, 034109 (2009)
39. B. Jaffe, W.R. Cook, H. Jaffe, *Piezoelectric Ceramics* (University of Michigan, R.A.N Publishers, Marietta, 1971)
40. V.Q. Nguyen, H.S. Han, K.J. Kim, D.D. Dang, K.K. Ahn, J.S. Lee, J Alloys Compd. **511**, 237–241 (2012)
41. V.D.N. Tran, A. Hussain, H.S. Han, T.H. Dinh, J.S. Lee, C.W. Ahn, I.W. Kim, Jpn. J. Appl. Phys. **51**, 0902 (2012)

42. V.D.N. Tran, H.S. Han, C.H. Yoon, J.S. Lee, J. Rödel, Mater. Lett. **60**, 2607–2609 (2011)
43. A. Hussain, C.W. Ahn, J.S. Lee, A. Ullah, I.W. Kim, Sens Acta A **158**, 84–89 (2010)
44. A. Hussain, A. Zaman, Y. Iqbal, M.H. Kim, J Alloys Compd **574**, 320–324 (2013)